Published in final edited form as:

Nat Biotechnol. 2018 August ; 36(7): 597–605. doi:10.1038/nbt.4162.

Human ESC-Derived Cardiomyocytes Restore Function in Infarcted Hearts of Non-Human Primates

Yen-Wen Liu[*,1,2,10], **Billy Chen**[*,1,2,5], **Xiulan Yang**[*,1,2,3], **James A. Fugate**[1,2,3], **Faith A. Kalucki**[1,2,3], **Akiko Futakuchi-Tsuchida**[1,2,3], **Larry Couture**[6], **Keith W. Vogel**[7], **Clifford A. Astley**[7], **Audrey Baldessari**[7], **Jason Ogle**[7], **Creighton W. Don**[5], **Zachary L. Steinberg**[5], **Stephen P. Seslar**[5,8], **Stephanie A. Tuck**[1,2,3], **Hiroshi Tsuchida**[1,2,3], **Anna V. Naumova**[1,2,9,11], **Sarah K. Dupras**[1,2,3], **Milly S. Lyu**[9], **James Lee**[5], **Dale W. Hailey**[1], **Hans Reinecke**[1,2,3], **Lil Pabon**[1,2,3], **Benjamin H. Fryer**[1,2,3], **W. Robb MacLellan**[1,2,5], **R. Scott Thies**[1,2,3], and **Charles E. Murry**[1,2,3,4,5]

[1]Institute for Stem Cell and Regenerative Medicine, University of Washington, Seattle WA 98109

[2]Center for Cardiovascular Biology, University of Washington, Seattle WA 98109

[3]Department of Pathology, University of Washington, Seattle WA 98109

[4]Department of Bioengineering, University of Washington, Seattle WA 98109

[5]Department of Medicine/Cardiology, University of Washington, Seattle WA 98109

[6]City of Hope, Beckman Research Institute, Duarte CA 91010

[7]Washington National Primate Research Center, University of Washington, Seattle WA 98195

[8]Department of Pediatrics, University of Washington, Seattle Children's Hospital, Seattle WA 98105

[9]Department of Radiology, University of Washington, Seattle WA 98195

[10]National Chen Kung University Hospital, Tainan, Taiwan

[11]Research Institute of Biology and Biophysics, National Research Tomsk State University, Tomsk, Russia

Abstract

Address for Correspondence: Charles E. Murry, MD, PhD, murry@uw.edu.

[*]**Equal contributions statement**

These authors contributed equally to this work.

Present addresses:

Yen-Wen Liu
Division of Cardiology, Department of Internal Medicine, National Cheng Kung University Hospital, College of Medicine, National Cheng Kung University, Tainan, Taiwan
Larry Couture
Orbsen Therapeutics, LTD, Orbsen Buildings, National University of Ireland Galway, Galway, Ireland, H91 DK 59
Stephanie A. Tuck
Uptake Medical Technologies, Seattle WA 98177

Competing Interest Declaration

Drs. Murry, Thies and MacLellan are scientific founders and equity holders in Cytocardia.

Pluripotent stem cell–derived cardiomyocyte grafts can remuscularize substantial amounts of infarcted myocardium and beat in synchrony with the heart, but in some settings cause ventricular arrhythmias. It is unknown whether human cardiomyocytes can restore cardiac function in a physiologically relevant large animal model. Here we show that transplantation of ~750 million cryopreserved human embryonic stem cell–derived cardiomyocytes (hESC-CMs) enhances cardiac function in macaque monkeys with large myocardial infarctions. One month after hESC-CM transplantation, global left ventricular ejection fraction improved 10.6±0.9% vs. 2.5±0.8% in controls, and by 3 months there was an additional 12.4% improvement in treated vs. a 3.5% decline in controls. Grafts averaged 11.6% of infarct size, formed electromechanical junctions with the host heart and by 3 months contained ~99% ventricular myocytes. A subset of animals experienced graft-associated ventricular arrhythmias, shown by electrical mapping to originate from a point-source acting as an ectopic pacemaker. Our data demonstrate that remuscularization of the infarcted macaque heart with human myocardium provides durable improvement in left ventricular function.

Heart disease kills more people worldwide than any other illness [1]. Much of this morbidity and mortality occurs because the heart is one of the least regenerative organs in the human body [2]. The ability of cardiomyocytes to proliferate is limited to ~1% per year [3–5], and it has been difficult to identify a cardiac stem cell population that can give rise to new myocytes at significant levels [3, 6]. As a result, cardiac injuries, such as myocardial infarctions, heal by scar formation, and the heart loses contractile ability in direct relation to the muscle deficit. When significant myocardial mass is lost, patients often progress to heart failure. Drug treatments for heart failure manage symptoms but do not address the root problem of muscle deficiency.

Over the last 20 years, there have been extensive efforts to induce the heart to heal by muscle regeneration rather than scarring [7–9]. Progress is being made on multiple fronts, including inducing cardiomyocyte proliferation [10–15] and reprogramming fibroblasts into cardiomyocytes [16–18]. Here we focus on transplantation of human cardiomyocytes derived from hESCs. These early-stage cardiomyocytes survive after transplantation and form new, maturing myocardium in animal models of myocardial infarction [19, 20]. They improve cardiac function when transplanted into the mouse [21], rat [22, 23] and guinea pig [24] infarct. A recent study from our group showed that hESC-CMs could remuscularize the infarcted hearts of macaque monkeys, where they formed electromechanical junctions with the host heart and beat in synchrony [25]. Although small-animal studies showed no evidence for arrhythmias, in monkeys hESC-CMs caused a transient period of ventricular arrhythmias[25]. Similar ventricular arrhythmias were reported when monkey pluripotent stem cell–derived cardiomyocytes were transplanted into infarcted monkey hearts [26].

The current study aimed to address two principal gaps in knowledge. The first was to learn whether hESC-CMs could restore contractile function in physiologically relevant large animals. For this we chose the non-human primate, *Macaca nemestrina*, because of their evolutionary proximity to humans, the similarity of their cardiovascular systems to humans, and because they are a well-established model in transplantation biology. This model should yield the best possible prediction of the human response to hESC-CM transplantation. The

second was to understand the physiological basis for the ventricular arrhythmias induced by hESC-CMs. We report here that hESC-CMs provide robust and durable improvement in cardiac function in the infarcted macaque heart. We also provide evidence that graft-induced arrhythmias result from pacemaker-like activity rather than abnormal conduction.

Results

hESC-CMs Improve Ventricular Function

The central hypothesis of this study was that hESC-CM would remuscularize the hearts of macaque monkeys and restore their function after myocardial infarction. To assess the impact of hESC-CM transplantation on left ventricular structure and function, we developed techniques for cardiac magnetic resonance imaging (MRI) in the macaque. MRI is currently the gold standard for non-invasive cardiac imaging of cardiac structure, function and tissue characterization. It provides reproducible measurements of left ventricular end-diastolic and end-systolic volumes (LVEDV and LVESV), cardiac output (CO), left ventricular ejection fraction (LVEF), regional wall thickening during systole and infarct size [27, 28]. Our previous study in macaques [25] created infarcts by occluding the distal left anterior descending (LAD) coronary artery for 90 min, followed by reperfusion. Pilot studies showed that this protocol gave a minimal reduction in ejection fraction, from ~65% at baseline to ~60% after infarction. For the functional studies here, we induced larger infarcts by occluding the mid-LAD for 3 hours, followed by reperfusion (Fig. 1a). This induced transmural infarcts (Fig. 1b; Suppl. Table 1) and reduced ejection fraction to ~40% two weeks after infarction (Fig. 1d, e), creating a greater window for detecting functional improvement.

With this new infarction protocol in place, we undertook an efficacy study. Electrodes for EKG telemetry were implanted at the time of infarction to assess spontaneous arrhythmias. Immunosuppressive agents were administered starting 5 days before cell delivery (Fig. 1a and Methods). Cells were administered ~14 days post-infarction by direct injection under surgical visualization. Cardiomyocytes were derived from the RUES2 hESC line in monolayer cultures using activin A and BMP4 to induce differentiation[22, 24, 25], or from the H7 hESC line in suspension cultures using small molecule Wnt pathway modulation to induce differentiation [29]. The 5 animals studied by MRI received cardiomyocytes derived from the H7 hESC line. Purity of the cultures averaged 86–99% cardiomyocytes, based on flow cytometry for cardiac troponin T (Suppl. Fig 1). We delivered ~750 million hESC-CMs or vehicle (RPMI/pro-survival cocktail [PSC]) by surgically exposing the heart and injecting intramuscularly into the infarct region and the border zones. MRI was performed one day prior to cell delivery and ~27 days after cell delivery, with all scans independently evaluated by 3 blinded observers. A subset of the animals underwent catheter-based electrophysiological studies at approximately day 14. Most macaques were euthanized ~28 days after cell transplantation, with the exception of two hESC-CM-treated and one control animal, which were given prolonged immunosuppression and studied by MRI at 12 weeks post-injection to assess durability of the functional effects.

Seventeen macaques initially were enrolled in this study without randomization, and another two were enrolled for targeted mechanistic studies, described below. Eight animals were excluded from final MRI analysis due to protocol design or complications outlined in Suppl.

Fig. 2, only one of which was related to cell treatment, but nine successfully completed the infarction, cell or vehicle injection, and multiple MRI scans (Fig. 1c). MRI scans were read by two blinded observers, with excellent inter-observer variability (Suppl. Fig. 3a).

Prior to infarction, LVEF was 69.8 ± 1.3% in the control group and 68.8 ± 2.1% in the hESC-CM group (Fig. 1d, e; P = NS). After infarction but prior to treatment, both groups exhibited similarly depressed LVEF, averaging 38.0 ± 2.3% in control animals and 39.4 ± 2.1% in hESC-CM-treated animals (p = NS). At 4 weeks post-treatment, transplantation of hESC-CMs significantly improved LVEF (hESC-CM *vs.* control: 50.0 ± 1.9 *vs.* 40.5 ± 2.2%, $p < 0.05$, Fig. 1d, e). The effects of hESC-CM transplantation also could be seen by comparing the change in LVEF between day −1 and day 27: the control group showed an improvement of 2.5 ± 0.8%, whereas the hESC-CM-treated group improved by 10.6 ± 0.9% ($p = 0.001$, Fig. 1f). To assess contractile function in the infarct zone, we measured systolic wall thickening. Prior to therapy, all animals had 0% systolic LV wall thickening in the infarct zone, and all control hearts had 0% systolic LV wall thickening at 4 weeks. In contrast, after hESC-CM transplantation, wall thickening in the infarct improved to 22.0 ± 12% of the LV wall (Fig. 1g). However because the improvement ranged from 0–67%, this was not statistically significant. Wall thickening in the non-infarcted region was not different between these 2 groups at any time (Suppl. Fig. 4), and there was no significant effect of cardiomyocyte transplantation on left ventricular end-diastolic volume. Taken together, these data indicate that formation of human myocardium in the infarcted non-human primate (NHP) heart improves LV systolic function.

To test for the durability of the functional benefit, we studied three macaques at 3 months post-engraftment (2 treated, 1 control; Figure 1h). In the control animal, the LVEF decreased from 43.9% at day 27 to 40.4% at 3 months. In the hESC-CM-treated animals, LVEF improved from 51.1% and 51.0% at day 27 to 66.0% and 61.0% at 3 months. Thus, the benefit from hESC-CM therapy appears to be durable for 3 months, with function improving between 1 and 3 months.

Ventricular Arrhythmia Analysis

To study spontaneous arrhythmias, we instrumented macaques that received 3-hour coronary occlusion followed by reperfusion with EKG telemetry systems. Cardiac rhythms were recorded continuously for 24-hour periods at 3-day intervals, and episodes of sustained ventricular tachycardia or accelerated idioventricular rhythm were quantified by one observer and validated by a second (Suppl. Fig. 3b). Representative EKG tracings of these rhythms are shown in Fig. 2a–d. A total of 6 hESC-CM-treated and 4 control animals successfully completed this phase of the study. Arrhythmias were quantified in hours/day and are shown for each animal in Fig. 2e, f. Compared to our previous study using the small infarct model with amiodarone anti-arrhythmic treatment [25], there were two notable differences. First, both groups showed significantly more arrhythmias prior to cell/vehicle injection. This could be due either to the larger infarcts or the omission of the amiodarone from the current study. Second, unlike the small infarct model, where cell-treated animals had more frequent arrhythmias than controls, there was no statistical difference in the number or duration of arrhythmias between the two groups either before or after injection.

The telemetry data were highly variable, however, and one macaque deserves individual mention. This cell-treated animal developed extensive ventricular arrhythmias, including both ventricular tachycardia and accelerated idioventricular rhythm (AIVR). The ventricular arrhythmias began ten days after cell injection and largely consisted of continuous (>20 hours/day), monomorphic, wide complex tachycardia and AIVR (Figure 2f, arrow). Although the animal was in no acute distress at any time, these arrhythmias were of sufficient severity that adequate MRI scans for functional studies were unattainable due to the high rate and irregularity. An arrhythmia of this duration was not observed in the control group. Despite the lack of statistical proof, we think that the most prudent interpretation is that 1 of the 6 cell-treated animals developed arrhythmias that likely were due to the hESC-CM graft.

The lower burden of engraftment arrhythmia in the current study could result from differences in the infarct model (large infarcts here), the cells (transgenic cells expressing the Ca^{2+} indicator GCaMP3 were used previously) or from unanticipated effects of the anti-arrhythmic drug, amiodarone [30], used previously. We therefore returned to the small infarct model and transplanted transgene-free cardiomyocytes and omitted amiodarone (N=1 each; Suppl. Fig. 5). The transgene-free and amiodarone-free animals experienced a high burden of ventricular arrhythmias, providing evidence that the lower burden of arrhythmias in this study resulted from the larger infarcts.

To further characterize the ventricular arrhythmias and to assess arrhythmia vulnerability, we performed catheter-based electrophysiology (EP) studies using the CARTO III mapping system. EP studies included programmed ventricular stimulation to induce arrhythmias, as well as activation and voltage mapping to characterize induced and spontaneous ventricular arrhythmias. We employed a standard programmed ventricular stimulation protocol, where a series of entrainment stimuli were followed by up to three extra stimuli, delivered in succession at coupling intervals down to the ventricular refractory period, with or without isoproterenol infusion. Arrhythmia inducibility and severity were graded as previously reported [31]. The proposed mechanism of the tachycardia was determined by electrophysiological features including cycle length stability, pacing inducibility, and susceptibility to pace or electrical cardioversion. In instances where there was spontaneous initiation, significant cycle length variation without change in VT morphology, and the inability to pace-induce or terminate with pacing or electrical cardioversion, the mechanism was presumed to be enhanced automaticity. In contrast, a relatively fixed cycle length and the ability to pace-induce, and susceptibility to pace or electrical cardioversion suggested a reentry mechanism.

Twelve EP studies were performed on 8 animals (3 control and 5 hESC-CM treated; 1 of the hESC-CM animals was from the small infarct protocol; Suppl. Fig. 2). Ten studies on 8 animals yielded data on arrhythmia inducibility. In 4 of these (3 hESC-CM treated, 1 control), ventricular stimulation resulted in induction of only brief episodes of non-sustained ventricular tachycardia and were thus unable to be mapped. In 2 EP studies (1 control and 1 hESC-CM treated), we induced ventricular tachycardia that caused significant hypotension, which precluded activation mapping and required termination with DC cardioversion. Quantitatively, there was no significant difference in arrhythmia inducibility between the

vehicle-injected and hESC-CM-injected hearts (Fig. 2g). Similarly, the severity of the induced arrhythmias did not differ between the hESC-CM-treated and control animals (Fig. 2g). Thus, intramyocardial injection of hESC-CMs did not increase the risk and the severity of inducible ventricular arrhythmias.

Activation maps of ventricular tachycardia were obtained in 2 hESC-CM treated and 1 control animal (Fig. 2h, i). In all cases, the ventricular tachycardia originated from a focal region. The control animal was studied twice, at 2 and 4 weeks post-injection, and in both studies the VT was induced, not spontaneous. In both studies the VT origin mapped to the low-voltage scar zone. The VT in the control heart was induced by pacing and could be terminated by overdrive pacing, both of which point to micro-reentry as the mechanism. Both cell-treated animals had spontaneous ventricular tachycardia when arrhythmia mapping began. These hearts could readily be overdrive-paced to 300 beats/min, but upon cessation of pacing, they returned almost immediately to their baseline tachycardic rates. We attempted to correct the arrhythmias with electrical cardioversion, but in both instances, after a brief pause the rhythm resumed at its previous rapid rate. Taken together, these data suggest the arrhythmias in control hearts arise from a small focus of reentry, whereas those in the hESC-CM have features of abnormal impulse generation.

Tumor Survey and Structural Analysis

One potential complication of hESC-CM therapy is teratoma formation or ectopic tissue growth [32]. All animals underwent a full necropsy by an experienced primate pathologist with a detailed gross and microscopic examination of the brain and all thoracic and abdominal organs. One cell-treated monkey had a microscopic focus of carcinoma in one kidney that was contained within small lymphatic and venous channels (Suppl. Fig. 6a, b). To test whether this tumor was of human or macaque origin, we performed in situ hybridization for human pan-centromeric genomic DNA sequences, and we also extracted DNA from the paraffin section for PCR genotyping. The tumor did not hybridize with the human-specific probe, and PCR detected only macaque DNA and was negative for human DNA (Suppl. Fig. 6c–f). This indicates that the tumor was of macaque origin. By immunohistochemistry, the tumor was negative for thyroid transcription factor-1 and GATA3. Conversely, it showed uniform, strong nuclear staining for Pax8. This immunophenotype is most consistent with a renal cell carcinoma[33]. No teratomas were detected in any animal, and no other atypical cellular masses were identified.

Histological analyses showed that infarcts in the sham-injected hearts averaged 23.6 ± 2.% of the LV mass, whereas 19.9 ± 1.1% of the LV was infarcted in hESC-CM-treated hearts (Fig. 3a; p=NS). We were able to obtain paired measurements of infarct size in 3 control and 5 hESC-CM–treated hearts at baseline and at 4 weeks post-engraftment using delayed gadolinium enhanced MRI (Fig. 3b; Suppl. Fig. 7). This showed greater scar shrinkage in the hESC-CM–engrafted infarcts (5.3 ± 0.2% vs. 2.3 ± 0.9% of the LV; $p<0.05$). This implies that the original infarct size was 25.9% of the LV in controls and 25.2% of the LV in hESC-CM–treated hearts.

To specifically label wild-type hESC-CMs in the graft, we identified two monoclonal antibodies to human grafts in the primate heart. The cardiac troponin I (cTnI) antibody is

human-specific, and the slow-skeletal troponin I (ssTnI) antibody recognizes the relatively immature human cells that still express this developmentally regulated isoform [34]. In archival hearts that had received GFP-expressing cardiomyocytes, these troponin antibodies labeled regions identical to those identified by immunostaining for GFP or via in situ hybridization for human pan-centromeric sequences (Suppl. Fig. 8). There was virtually no staining of macaque cardiomyocytes with either antibody. One macaque damaged its intravenous catheter, resulting in interruption of immunosuppression at 5 weeks post-transplantation in a planned 3-month survival protocol. No graft was detected in this animal, presumably due to rejection, and it was excluded from graft size calculations. In all other animals, large grafts of human myocardium were readily identified. Grafts ranged from 5.7–15.6% of the infarct (11.6 ± 2.3%; Fig. 3d) and 1.1–3.4% of the LV (2.2 ± 0.7%; Fig. 3c). In control hearts the infarct was a transmural scar, with subendocardial sparing of the host myocardium and significant wall thinning (Fig. 3f). In hESC-CM hearts, large grafts were readily identified, often measuring more than a centimeter in greatest dimension (Fig. 3g). Grafts were located in the central infarct region and in the border zone myocardium, suggesting little migration occurred from the original injection sites. Representative low-magnification images for 4 different engrafted hearts are presented in Suppl. Fig. 9. We estimated the number of cardiomyocytes in the grafts using histomorphometry (Figure 3e; see Methods). At 4 weeks post injection there were 21.7 and 83.9 million cardiomyocytes in the grafts. At 3 months there were 109 and 126 million cardiomyocytes in the grafts, suggesting expansion due to proliferation.

At 4 weeks post-engraftment, 90% of graft cells were definitive ventricular cardiomyocytes ($MLC2v^+/MLC2a^-$; Fig. 3h–j), and 10% typed as either atrial, sinoatrial or immature ventricular cardiomyocytes ($MLC2a^+/MLC2v^-$); only rare double-positive cells were identified. By 3 months post-transplantation, 99% of graft cells were $MLC2v^+$, with <1% still expressing MLC2a. This indicates that the vast majority of cardiomyocytes generated by the differentiation protocol used in this study adopt a ventricular phenotype after transplantation, although expression of MLC2v is time-dependent.

Cardiomyocyte grafts showed significant maturation *in vivo*. At 4 weeks post-transplantation (Fig. 4a) the cardiomyocytes were relatively small, had myofibrils principally at the cell periphery, and their alignment was disheveled. Additionally, the junctional proteins N-cadherin and connexin43 were circumferentially distributed (Suppl. Fig. 10). At 3 months, the cardiomyocytes were larger, had myofibrils throughout the cytoplasm and were better aligned (Fig. 4b). N-cadherin was often polarized to intercalated disk-like structures, whereas connexin43 remained circumferentially distributed, though to a lesser extent than at 4 weeks (Suppl. Fig. 10). Additionally, by 3 months the hESC-CMs had readily discernible caveolin 3^+ invaginations of the sarcolemma that likely represent T tubule networks (Fig. 4c). Although relatively immature, the 4 week grafts already had begun switching from the fetal ssTnI to the adult cTnI isoforms (Fig. 4a). Increased intensity of cTnI staining was readily apparent at 3 months (Fig. 4b), again indicating maturation. Areas of electromechanical integration were readily identified in all hearts where hESC-CMs formed N-$cadherin^+$ adherens junctions and $connexin43^+$ gap junctions with host cardiomyocytes (Fig. 4d–g).

Grafts had an extensive network of $CD31^+$ blood vessels (Fig. 4h, i), indicating vascularization by the host coronary circulation. At 4 weeks, grafts averaged 406 ± 11 vessels/mm^2, and this increased to 576 ± 4 vessels/mm^2 at 3 months, likely reflecting ongoing angiogenesis. In contrast, the infarct scar around the graft showed a time-dependent decline in vascular density, from 450 ± 40 vessels/mm^2 at 4 weeks to 284 ± 58 vessels/mm^2 at 3 months. Vascular density in the remote myocardium did not change over time, averaging 1034 ± 1.2 and 1043 ± 2.5 vessels/mm^2 vessels/mm^2 at 4 weeks and 3 months, respectively.

Graft cardiomyocyte proliferation was measured by double staining for pericentriolar material-1 (PCM-1) and Ki67. PCM-1 marks the outer perimeter of cardiomyocyte nuclei [35], and Ki67 is a pan-cell cycle epitope. Graft cell proliferation was detected in all hearts (Fig. 4j, k). At 4 weeks, graft cardiomyocyte proliferation rates were 10.3% and 3.5%. At 12 weeks, the proliferation rates were 2.6% and 3.5%. This demonstrates that significant cell cycle activity occurs in the grafted cardiomyocytes, and coupled with the measured increase in graft cell number between 4 and 12 weeks, suggests that these are complete cell divisions rather than increases in ploidy.

The large size of these grafts made visualization by cardiac MRI possible. Using delayed-gadolinium enhancement, three animals showed the appearance of islands of new tissue (viable Gd-negative tissue) within the infarcted anterior wall and septum at 1 and 3 months after treatment (Fig. 5a–c). These islands were ~1 cm in maximal dimension. By carefully cross-registering histology and MRI scans, we identified regions of human myocardium, > 1 cm in maximal dimension, that corresponded to these Gd-negative regions in the MRI images (Fig. 5d, e). Masses of this size are easily visualized by MRI, leading us to conclude that it is possible to image large-scale regeneration from hESC-CM grafts.

Discussion

A long-term goal of our program is to remuscularize the heart after myocardial infarction, and thereby improve its function. We have shown here that hESC-CMs can remuscularize infarcts in macaque monkey hearts and, in so doing, reduce scar size and restore significant levels of cardiac function. The infarcts studied were large, reducing ejection fraction from 69% to ~40%. No significant spontaneous recovery occurred in the vehicle-injected group (~2.5%), whereas all hESC-CM–treated hearts showed significant recovery at 4 weeks (10.6 ± 0.9%). Based on studies on three macaques extended to 3 months, the benefit to cardiac function appears durable, with further functional improvement between 1 and 3 months. Although pluripotent stem cell derivatives can cause teratomas [32, 36, 37], none were observed in the current study.

The 20% absolute improvement in LVEF seen in the 2 hESC-CM hearts studied at 3 months was striking and shows that substantial mechanical improvement can occur between 1 and 3 months. Shiba et al [26] also found significant improvement in LVEF after transplantation of allogeneic macaque iPSC-derived cardiomyocytes into macaque infarcts[26]. The mechanical benefit could, in principle, result from direct mechanical force from the graft and/or paracrine signals [38] that enhance function of the host myocardium. We have shown that hESC-CM grafts form gap junctions with host myocardium and beat in synchrony in rat,

guinea pig and primate hearts [24, 25, 39]. The fact that grafts in the present study are large and beat in synchrony with host myocardium is consistent with a direct contribution to contractile function, as are the increased hypertrophy and maturation of engrafted cardiomyocytes. There also is evidence for paracrine effects of human pluripotent stem cell derivatives in the heart. Zhu et al [40] recently reported that hESC-derived cardiac progenitors enhanced function of non-human primate hearts, even though the cells were rejected. That study differed from ours in many ways, including giving progenitors instead of definitive cardiomyocytes, using a dose that was ~1% of ours, delivering cells immediately after a permanent coronary occlusion instead of 2 weeks after ischemia-reperfusion, and using an immunosuppression regimen that did not prevent rejection. Tachibana et al [41] found that hESC- and hiPSC-derived cardiomyocytes could enhance function of the infarcted mouse heart with minimal engraftment, and they also attributed this benefit to paracrine signaling. These two papers demonstrate that human cardiac progenitors and cardiomyocytes can have benefits through indirect, paracrine mechanisms.

A major goal of this study was to understand the basis for ventricular arrhythmias associated with human cardiomyocyte engraftment. Mouse ESC-derived cardiomyocytes grafted into the infarcted mouse heart led to increased spontaneous arrhythmias [42, 43] yet decreased susceptibility to pacing-induced arrhythmias [44]. When human ESC-CMs were transplanted into injured guinea pig hearts, our group found no effects on spontaneous arrhythmias and reduced susceptibility to pacing-induced arrhythmias [24]. In contrast, hESC-CMs transplanted into the hearts of macaque monkeys with small infarcts induced transient ventricular arrhythmias [25, 45]. Similar arrhythmias were noted when allogeneic monkey iPSC-derived cardiomyocytes were transplanted into infarcted monkey hearts [26]. The similarity of arrhythmias in that allogeneic model and our xenogenic model suggests that species-incompatibility is not the basis for arrhythmias in our model.

Although graft-induced arrhythmias appear to be less frequent in the large infarct model used here, at least one of our cell-treated macaques experienced ventricular arrhythmias that can reasonably be attributed to the graft. This raises the possibility that similar arrhythmias could occur in humans treated using the same protocol. We systematically ruled out effects from the GCaMP transgene and the amiodarone drug treatment used in our previous study. Although we hypothesized that hESC-CM grafts were creating tracts of slow conduction leading to re-entrant arrhythmias, this was not supported by the data. In electrical mapping studies, no re-entrant pathway could be identified; rather, the impulse appeared to originate from a point-source in the graft region. This indicates either an ectopic activation source or a re-entry pathway smaller than the resolution of our mapping (~1 cm). The arrhythmia could not be extinguished either by overdrive pacing or by electrical cardioversion, both of which favor ectopic impulse generation. Finally, there was no difference in susceptibility of the engrafted hearts vs. the vehicle-injected hearts to arrhythmias induced by programmed electrical stimulation, which typically elicits reentrant arrhythmias in regions of abnormal conduction. All these characteristics point toward a disorder of impulse generation (either pacemaking or after-depolarizations) rather than reentry as the underlying cause for hESC-CM–induced arrhythmias. These insights may help identify pharmacological or cell-autonomous interventions to limit arrhythmias in the future.

There are several limitations to this study. First, because it is a primate study, group sizes are smaller than is typical for a small animal study. Although we demonstrate statistically robust data for mechanical improvement, some experiments showed trends that would require larger groups for statistical significance. This is mitigated in part by the high animal-to-animal consistency in physiological responses. Second, this xenotransplantation study does not address the human immune response to allogeneic cardiomyocytes. While testing human cardiomyocytes is essential for regulatory approval, allogeneic data from monkeys would be useful.

The functional recovery seen in the current study was larger than we have observed using rat [22] or guinea pig [24] models of myocardial infarction, even though grafts occupied a similar fraction of the ventricle. This finding is likely explained by that the greater physiological match between human and macaque. The therapeutic effect may be further augmented when human cardiomyocytes are transplanted into diseased human hearts.

Online Methods

To enhance transparency and reproducibility, a Life Sciences Reporting Summary for this manuscript is available from the Nature Biotechnology website.

Cell preparation

These studies were approved by the University of Washington Stem Cell Research Oversight Committee. Two lines of hESCs were used in this study. RUES2 cells (obtained from Rockefeller University) were expanded in monolayers in mouse embryonic fibroblast-conditioned medium. Differentiation was performed by replating the cells in high density monolayers, followed by sequential treatment with recombinant human activin A and BMP4, as previously described [22, 24, 25, 46]. Prior to cryopreservation, RUES2-derived cardiomyocytes were heat-shocked and treated with a pro-survival cocktail to enhance their survival after transplantation [22, 25, 46]. H7 hESCs (obtained from WiCell) were cultured, expanded, and differentiated in suspension-culture format by collaborators at the Center for Applied Technology Development at the City of Hope in CA[29]. Pluripotent H7 cultures were expanded in the commercially available media, StemPro hESC SFM. For cardiac differentiation pluripotent aggregates were cultured in RPMI-1640 supplemented with B-27® (with or without insulin). Differentiation is induced by treatment with the small molecules Chir99021 and IWP-4. On day 21 of differentiation, cardiomyocyte aggregates were dissociated by treatment with Liberase TH and TrypLE. Dissociated CMs were cryopreserved in CryoStor CS10 supplemented with 10 μM Y-27632 with freezing performed in a controlled-rate liquid nitrogen freezer. Four lots of H7-cardiomyocytes were received by dry ice shipment, and stored in LN2 prior to use. Two lots of cardiomyocytes were thawed and blended in approximately equal numbers to produce consistent cell treatments for each of the five treated animals completing the study. Per the City of Hope Product Summary, cryopreserved cells and thawed cells were a mean average 96% cTnT positive and 85% viable. Following shipment and additional storage time thawed cells were shown to be 86% viable using an NC200/ Via1-cassette™ (Chemometec, Denmark) and 87% cTnT positive (human IgG anti-cardiac troponin clone REA400; Miltenyi, Germany).

Approximately 3 hours before transplantation, cryopreserved cardiomyocytes were thawed in a 37°C water bath (2 minutes ± 30 seconds). RPMI-1640 supplemented with B-27® and ≥200 Kunitz Units/mL DNase I was added to the cell suspension to dilute the cryopreservation media. Subsequent wash steps were done using RPMI-1640 basal media in progressively smaller volumes in order to concentrate the cell suspension.

Before the last centrifugation step, the cell pellet was resuspended in a 5-factor Pro-Survival Cocktail (PSC). PSC consists of RPMI-1640 basal media supplemented with: 10μM ZVAD-FMK/Caspase Inhibitor (Calbiochem/EMD-Millipore); 50nM TAT-BH4 / BCL-XL (Calbiochem/EMD-Millipore); 200nM Cyclosporine A (Sandimmune/Novartis); 50μM Pinacidil (Sigma); and 100ng/ml IGF-1 (Peprotech). Unlike many of our previous studies, no Matrigel was used to deliver the cells.

After resuspension in PSC, the cell suspension was centrifuged so that sufficient volume of PSC supernatant can be removed in order to achieve a target cell density for injection (~7.5×10^8 cells in ~1.5 mL PSC). The final volume of the cell suspension was determined by the results of a count sampled prior to the final centrifugation step. Note that our previous study counted cells prior to the freezing step. Because there is a 25% cell loss after the thaw, this dose of 750 million cells is comparable to our previously reported dose of 1 billion [25].

Animal models

All procedures complied with and were approved by the University of Washington Animal Care and Use Committee.

Non-human primate catheterization and surgery

Macaca nemestrina monkeys of either sex, weighing 5.2–12.6 kg, were obtained from the Washington National Primate Center. Ages are specified in Table 1. Macaques first underwent a 2–4 week period of acclimation and training to wear a mesh jacket with an exteriorized line that attached to a tether system to prevent removal of intravenous (i.v.) catheter and EKG electrodes. For all major surgeries and procedures, macaques were sedated with ketamine and propofol, intubated and ventilated using sevoflurane or isoflurane to maintain anesthesia. Buprenorphine SR was administered to provide perioperative and postoperative pain relief.

Before myocardial infarction creation, an i.v. lidocaine bolus of 1mg/kg and an infusion of 20 μg/kg/min were used to prevent ventricular arrhythmias. Heparin was delivered i.v. to maintain activated clotting times (ACT) of 250–350 s to prevent thrombus formation. Femoral artery access was obtained via direct cutdown followed by puncture with a 5F Terumo Glidesheath. Under fluoroscopic guidance (OEC 9800 Plus, GE Medical Systems), a 5F Convey guiding catheter (a modified FL3, Boston Scientific) used to engage the left main coronary artery (LAD). A coronary guide wire and angioplasty balloon (Apex 2×8 mm PTCA Dilatation Catheter, Boston Scientific) were passed into the mid-left anterior descending artery. The balloon was inflated until the artery was occluded (as demonstrated by angiography) and left inflated for 180 min. Myocardial ischemia was confirmed by ST-segment elevation on EKG.

For telemetric monitoring, tunneled subcutaneous EKG electrodes were implanted (2 in the chest wall and 1 in the abdomen; lead II equivalent) and connected to wireless Vetcheck modules (Vmed Technology) through the jacket/tether system. Dual lumen venous catheters were implanted and tunneled to allow peripheral blood sampling and intravenous drug administration with minimal distress to the animals. Immune suppression was achieved with three drugs. Methylprednisolone was given i.v. 30 mg/kg on the day before hESC-CM delivery, followed by maintenance doses of 6 mg/kg for two days, and then 3mg/kg thereafter until monkeys were euthanized. Cyclosporine A was given i.v. to maintain serum trough levels of 200–250 μg/L from 5 days before hESC-CM delivery until macaques were euthanized. Finally, Abatacept (CTLA4-Ig) 12.5 mg/kg was administered subcutaneously on the day before hESC-CM and every 2 weeks thereafter. Ceftazidime, cefazolin, vancomycin, gentamycin, fluconazole, and acyclovir were administered for prophylaxis of opportunistic infections.

On approximately day 14 after myocardial infarction, macaques were anaesthetized and underwent left-sided thoracotomy. The heart was exposed and a pericardial cradle created. The infarct region was directly visualized, and hESC-CMs were delivered from an epicardial approach into the infarct and peri-infarct region via 15 injections each of 100 μl volume. Needle tips were placed within a preformed mattress suture, and three injections were delivered via the same epicardial puncture, changing the trajectory of the needle for each. Before withdrawal of the needle, the mattress suture was cinched around the needle tip to facilitate cell retention. For control macaques, an equal volume of PSC vehicle was injected in the same manner as for hESC-CM delivery. Three injections were place in the peri-infarct border zone, and two were placed into the central ischemic region. LAD coronary occlusion infarcts both the anterior free wall and the anterior 2/3 of the interventricular septum. Although the free wall is readily accessed from an epicardial approach, the septal wall is not visible. We targeted cells to the septum by passing the needle under the LAD artery and inferring the septal wall's location from the curvature of the left ventricular free wall.

Animals were regularly monitored by laboratory and Primate Center Staff. Euthanasia was induced under deep anesthesia by i.v. injection of saturated KCl. Control and cell-treatment groups were allocated in an un-blinded and non-randomized manner.

Post-surgery care

Post-infarct animals were monitored daily with particular attention paid to signs of distress, which may indicate post-procedure pain or symptoms of heart failure. If necessary, furosemide was injected to relieve pulmonary congestion or limb edema. Signs of distress, such as increased respiratory rate and crackles on auscultation of the chest were used to assess signs of pulmonary congestion. Surgical wounds were carefully examined for signs of infection. In the event of possible infection, wound swabs were obtained and sent for microbiology with the commencement of empirical antibiotics in consultation with veterinary staff. If there were any severe complications noted in the animal, we consulted the veterinarian staffs and treated as clinically appropriate. If the clinical or attending veterinarian diagnosed an untreatable complication (lower extremity ischemia, renal and liver failure, femoral artery dissection), the animal was euthanized. All animals had full

necropsies performed by an experienced primate pathologist. Individual procedure notes for each animal are available in the Online Appendix.

Cardiac MRI

Cardiac MRI was performed prior to cell injection (2 weeks after MI) and at 4 and 12 weeks post cell-injection. *In vivo* imaging studies were conducted on a 3-Tesla Achieva clinical scanner (Philips, Best, Netherlands). Depending on the animal size, two overlapped Flex-M and Flex-L coils (dual-element, approximately 15 and 20 cm diameter, respectively) or an 8-element knee coil was used. Pediatric EKG leads were used for gating of MRI acquisitions. EKG, respiration rate, arterial oxygen saturation and body temperature were monitored continuously.

The cardiac MRI protocol included CINE imaging for assessment for the LV geometry, global LV contractile function, regional systolic LV wall thickening and delayed gadolinium enhanced imaging for assessment of the infarct size. CINE images were acquired with a RF-spoiled turbo field echo (T_1-TFE) sequence that generated 25–30 cardiac phases for 10–12 short axis slices spanning the left ventricle. Acquisition parameters included a repetition time (TR) 3.9 msec, echo time (TE) 1.9 msec, a 15° flip angle (FA), 4 mm slice thickness (no gap), field of view (FOV) 120×120 mm^2, 1 mm^2 voxel size, 6–8 signal averages, retrospective EKG gating without breath hold.

Animals subsequently received an intravenous bolus injection of gadolinium-based contrast agent ProHance (Bracco Diagnostics Inc., Princeton, NJ) 0.2 mmol/kg, followed by a saline flush. At approximately 8 minutes after injection, inversion time (TI)-scout images were acquired for determination of TI to null signal from non-infarcted myocardium. At nine minutes post-injection of contrast agent, phase-sensitive inversion recovery (PSIR) multislice images were acquired at the LV short axis to visualize the infarct: TR/TE 7.3/3.5 msec, FA 25°, voxel size 1.3 mm^2, FOV 150×150 mm^2, slice thickness 4 mm without gap, four averages. This was repeated in the long axis plane. Inversion time ranged from 280–350 msec, adjusted by the operator based on TI-scout values. Signal intensity threshold to differentiate normal myocardium from scar was set as ‘Full Width Half Max’.

All MRI scans were analyzed by 3 independent reviewers who were blinded as to treatment and timing of the evaluations. Inter-observer variability was good, with an intraclass correlation coefficient of the average LVEF measurements was 0.978 (95% confidence interval [CI]: 0.951 – 0.990, $p < 0.001$; Suppl. Fig. 3a, b). Because within-reviewer variance was lower than the pooled variance, quantitative data from a single reviewer (AN) were used for all figures and tables. Pooled vs. single-reviewer analysis had no impact on statistical significance or the overall magnitude of changes observed. Global LV contractile function and regional wall thickness data were computed from the short-axis cine images. LV endocardial boundaries were traced at end-diastole and end-systole using standard cardiac analysis software (Intellispace Portal, Philips, Best, Netherlands) to obtain end-systolic, end-diastolic volume, LV myocardial mass (LVmass), stroke volume (difference between end-diastolic and end-systolic volumes), cardiac output (CO) and LV ejection fraction (LVEF). LVEF was calculated as the ratio of stroke volume to end-diastolic volume. Papillary muscles were excluded from the volume calculations. Left ventricle wall thickening (LVTh)

was calculated as relative difference in LV wall thickness in end-systole and end-diastole, divided by end-diastolic thickness. LVTh was evaluated at the infarcted and non-infarcted areas of the each slice of the heart. Infarct size was calculated from delayed Gd enhanced images and presented as the ratio of scar area to total LV area.

Echocardiography

Baseline transthoracic echocardiography was performed prior to infarct surgery to evaluate the animals' cardiac function. Macaques were sedated with ketamine and propofol and then were examined in the supine position, using a commercially available ultrasound system with a 5 MHz probe (Vivid-q, GE Healthcare, Horten, Norway). Apical four-chamber views were collected for baseline left ventricular ejection fraction (LVEF) measurement. Quantification of LVEF was performed by a qualified cardiologist according to the recommendation of the American Society of Echocardiography.

Telemetric EKG

EKG recordings were acquired from conscious, freely mobile animals using a Vmed Vetcheck telemetry system. Animals had tunneled subcutaneous EKG wires implanted, providing lead II tracings. Continuous telemetry was sent wirelessly to a dedicated laptop for all macaques with myocardial infarction with or without hESC-CM delivery on post-myocardial infarction days 1, 4, 7, 10, 13 and post-intramyocardial injection days 3, 6, 9, 12, 15, 18, 21, 24 and 27. All EKG traces were evaluated manually by a cardiologist (YWL) using EKG Reviewer (Vmed), and determined the total number and duration of ventricular arrhythmias. A second cardiologist evaluated a subset of these telemetry tracings in a blinded manner, with excellent concordance (Suppl. Fig. 3c). Premature ventricular complexes (PVCs) were defined as QRS complexes greater than 60ms. Ventricular tachycardia (VT) was defined as a run of four or more PVCs with ventricular rate of more than 180 beats per minute. Accelerated idioventricular rhythm (AIVR) was defined as four or more PVCs with a rate of less than 180 beats per minutes. VT or AIVR were considered sustained if the duration was greater than 30 seconds.

Histology and immunohistochemistry

Histological studies were carried out as detailed previously [19, 25] with some adaptation. Paraformaldahyde-fixed macaque hearts were dissected to remove the atria and right ventricle before cross-sections were obtained by sectioning parallel to the short-axis at 2.5 mm thickness on a commercial slicer (Berkel). Weights of the whole heart, left ventricle and each slice were obtained before cutting heart slices to fit tissue cassettes. The tissue then was processed, embedded in paraffin, and four-micrometer sections were cut for staining. For morphometry, infarct regions were identified by Picrosirius red staining; human grafts were identified by anti-human cardiac troponin I, stained using avidin-biotin reaction (ABC kits from VectorLabs) followed by chromogenic detection via diaminobenzidine (Sigmafast, Sigma Life Science). The slides were digitized using a Hamamatsu Nanozoomer whole slide scanner, and the images were viewed and exported with NDP software (NDP.view 2.6.13). Resulting images were imported into Image J software (version 1.51k) where area of infarct and graft (region of interest or ROI) were measured. The mass of the ROI was determined by calculating the ratio of ROI area to total tissue area on the slide, and multiplying by the

weight of the tissue the slide was cut from. The entire scar or graft was expressed as total weight or percent of LV mass.

For immunohistochemistry, we used the primary antibodies listed in Supplementary Table 2. Primary antibodies then were followed either with fluorescent secondary antibodies (Alexa-conjugated, species-specific antibodies from Molecular Probes) or the avidin biotin reaction (ABC kits from VectorLabs) followed by chromogenic detection via diaminobenzidine (Sigmafast, Sigma Life Science). Immunofluorescent images were collected with either a Nikon A1Confocal System or a Nikon Ti-E inverted widefield microscope. For high-resolution confocal images, a 60X CFI Plan Apo Water immersion objective lens (NA 1.2) was used. 12-bit images were captured with the pinhole at 1 Airy Unit and field size at 1,024 X 1,024 pixels. For large field immunostained sections, a CFI Pan Apo lambda 4X objective (NA 0.2) was used on the widefield system. Grids of 14-bit Images were captured using a Photometrics CoolSnap HQ2 CCD camera and stitched with NIS Elements version 5.00 software. For figure preparation, images were exported into Photoshop CS3 (Adobe). If necessary, brightness and contrast were adjusted for the entire image and the image was cropped.

Histomorphometry

Infarct size was determined from whole-slide scans of picrosirius red-fast green stained tissue sections. Infarct size was calculated as Σ(block mass × infarct area/block area) and expressed as a percentage of the left ventricular mass.

Graft size was determined from whole-slide scans of sections stained with human-specific cTnT. Graft size was calculated as Σ(block mass × graft area/block area) and expressed either as a percentage of the left ventricular mass or the infarct mass.

Vascular density was determined from photomicrographs of CD31-stained sections from the graft, scar and remote (non-infarcted) myocardium obtained with a 40X objective. A defined-area grid was overlaid onto the image, and vascular profiles within a region of interest were counted. Vessels that crossed into multiple grid subunits were counted only once. Vascular density is expressed as the number of vessels/mm^2.

Graft cardiomyocyte number was estimated from photomicrographs of sections stained with pericentriolar material-1 (PCM-1). Regions of interest shown to contain no host cardiomyocytes in adjacent sections were photographed with a 40X objective. A defined-area grid was overlaid onto the image, and PCM-1^+ nuclear profiles with clear rings of perinuclear staining were counted. To determine the number of microscopic fields required, we performed a systematic downsampling study. Counting 42, 25, 10 and 5 fields yielded cardiomyocyte densities of 3865, 3848, 3934 and 3858 nuclei/mm^2. Subsequent studies were done with 5 fields per heart. To calculate graft cardiomyocyte nuclear density on a volume basis, we made the assumption that the nuclei were isotropically packed, i.e. that the densities in the XY, XZ and YZ planes were equivalent. (This was supported by microscopic observation that linear nuclear densities in the X and Y dimensions were comparable.) Volume-based nuclear density was calculated as $(\text{nuclei/mm}^2)^{1.5}$, yielding nuclei/$mm^3$. Finally, because our grafts are relatively immature, we made the assumption that each

cardiomyocyte is mononucleated, meaning that nuclear density = cardiomyocyte density. (Note that even in adult human myocardium, only 25% of cardiomyocytes have more than 1 nucleus [ref [2]], so the impact of this assumption is modest.) Total graft number was determined as:

$$total\ graft\ cardiomyocyte\ number = \frac{graft\ cardiomyocyte\ number}{mm^3} \cdot \frac{graft\ mass\ (mg)}{tissue\ density\ (1.06\frac{mg}{mm^3})}$$

The proliferation rate of engrafted cardiomyocytes was determined from sections stained for PCM-1 and Ki67. Regions of interest shown to contain no host cardiomyocytes in adjacent sections were photographed with a 40X objective. Cardiomyocyte nuclei were identified by a clear perinuclear ring of PCM-1 staining. The number of cells counted ranged from 607 to 1341 per heart. The proliferation rate is expressed as 100X[the number of PCM-1^+/Ki67^+ double-positive nuclei] divided by the number of PCM-1^+ nuclei.

In situ hybridization

Engrafted human cells were identified using in situ hybridization with a human-specific pan-centromeric genomic probe as previously reported [4] and used to validate human specific antibodies. In brief, the human-specific pan-centromeric probe was generated by modification of a protocol previously reported [7] that involves degenerate PCR with primers against human alpha satellite pan-centromeric repeat sequences. PCR was performed for 30 cycles: denaturation at 94°C for 1 minute; annealing at 45°C for 1 minute; extension at 72°C for 1 minute. We then labeled the PCR product with biotin (Biotin DecaLabel DNA kit, Thermo Scientific) to generate the in situ probe. The pan-centromeric probe was diluted in hybridization buffer (0.5× SSC, 10% dextran sulfate, 50% deionized formamide, 0.4mg/mL salmon sperm DNA), heated to 80°C to denature the DNA, applied to the slide and hybridized overnight at 37°C. Subsequent detection after in situ hybridization utilized peroxidase-conjugated avidin (ABC kits from VectorLabs). For immunohistochemistry, the in situ probe was detected by Alexa Fluor 594 tyramide amplification (Molecular Probes).

PCR detection of human DNA

One of the hESC-CM treated animals had a renal tumor identified during necropsy. Human and macaque specific primers were used to determine that the tumor was not human tissue. Genomic DNA was isolated from adjacent slices (with respect to pan-centromeric probe section) using a Qiagen DNeasy tissue kit and 250 ng of input gDNA per sample was used for PCR. Human (HS) and macaque (MN) gDNA was used as controls.

To detect human DNA, we made primers targeting human mitochondria: forward primer 5′-CACCGGCGCAGTCATTCTCATA-3′ and reverse primer 5′-GAGTCCTGTAAGTAGGAGA-3′. PCR profile: 95°C/1 minute, 59°C/1 minute, 72°C/1 minute for 40 cycles, product size 267 bp. Human specific primers detect a 249 bp region on human mitochondria DNA (11680–11929; MF992925.1).

For macaque-specific PCR, we developed primers targeting chromosome-3: forward primer 5′-CAGTTGGCTGTTCAGTATAGCGAT-3′ and reverse primer 5′-

CTTCAGAGTATGTGACATAGGT-3′. PCR profile: 95°C/1 minute, 55°C/1 minute, 72°C/1 minute for 40 cycles, product size 150 bp. Macaque specific primers detect a 150 bp region on macaque chromosome 3 (8392421–8392571; LT160002.1).

Electrophysiology studies

To determine inducibility and mechanism of ventricular arrhythmias, macaques underwent catheter-based electrophysiology study. The animals were sedated with ketamine and propofol and intubated. Anesthesia was maintained with sevoflurane. Heart rate, non-invasive blood pressure, and pulse oximetry monitors were connected. R2 pads were placed and connected to a defibrillator. Depending upon the animal and prior vascular access, either the left or right femoral artery was accessed using a hybrid cut down / Seldinger technique. A 7 French hemostatic sheath was placed into the femoral artery. Through this sheath a CARTO NaviStar B-curve, D-curve, or a PENTARAY (Biosense Webster Inc, Diamond Bar, CA) catheter was placed and advanced retrograde through the aortic arch into the left ventricle. If the macaque was in sinus rhythm at the onset of the study, a substrate map was created in sinus rhythm and areas of low voltage annotated. Scar was defined as a voltage of <0.5 mV and / or inability to capture the myocardium at a pacing output of 10mA at 2ms pulse width. Diseased myocardium was defined by a voltage of 0.5 – 1.5 mV, and healthy myocardium > 1.5 mV. Following substrate mapping, a ventricular stimulation protocol was performed with an 8-beat drive train with single, double, and triple extrastimuli down to the ventricular effective refractory period. The protocol was repeated at 2 sites and 2 drive train cycle lengths. If non-inducible under baseline conditions, the protocol was repeated on an isoproterenol infusion titrated to achieve a 25% increase in baseline heart rate. Inducibility and severity were graded using the scales presented in Suppl. tables 3 and 4.

For induced and spontaneous ventricular arrhythmias, electroanatomic and voltage mapping was performed. The arrhythmia was characterized as focal if there was radial spread of electrical activation from a point source and macro-reentrant if there was an identified circuit of electrical activity with an early-meets-late activation pattern. Activation mapping was performed using the CARTO III system with either a 7-French NaviStar B- or D-curve catheter or a 7-French D-curve PENTARAY catheter (Biosense Webster Inc, South Diamond Bar, CA, USA).

Statistical analysis

All values are expressed as mean ± SEM. Paired t-tests and 2-tailed t-tests were performed using Graphpad Prism software, with the threshold for significance level set at $P<0.05$.

Animal Care and Procedure Notes

General Features of Primate Care Following Infarction and Cell Therapy

Post-infarct animals were monitored daily with particular attention paid to signs of distress, which may indicate post-procedure pain or symptoms of heart failure. If necessary, furosemide was injected to relieve limb edema or pulmonary congestion, manifest as increased respiratory rate and crackles on auscultation of the chest. Dobutamine infusion was started for clinical signs of poor end-organ perfusion in the setting of heart failure or

cardiogenic shock. In the event of frequent PVCs or AIVR on telemetry, a short course of lidocaine infusion was given. For any hemodynamically unstable arrhythmias, the animals would undergo the normal algorithm of advanced cardiovascular life support.

Surgical wounds were carefully examined for signs of infection. In the event of possible infection, wound swabs were obtained and sent for microbiology with the commencement of empirical antibiotics in consultation with veterinary staff. If there were any severe complications noted in the animal, we consulted the veterinarian staffs and treated as clinically appropriate. If the clinical or attending veterinarian diagnosed an untreatable complication, the animal was euthanized. All animals had full necropsies performed by an experienced primate pathologist.

Procedure Notes

P11—The angioplasty balloon was inflated for a total of 90 minutes for ischemia. After about 40 minutes of ischemia, the animal had several premature ventricular complexes (PVC's) leading to non-sustained episodes of ventricular tachycardia (NSVT) lasting up to 30 seconds, with associated hypotension. The NSVT self-converted back to normal sinus rhythm and normal blood pressure. No electrical cardioversion was attempted. Lidocaine infusion was initiated (20ug/kg/min), a bolus of MgSO4 (0.25mg) was given. No arrhythmia was noted after balloon deflation and reperfusion. Lidocaine infusion was continued for 1 day after infarct surgery.

P12—Balloon placement for infarction for this animal was in the proximal LAD for 90 minutes. Inflation of the balloon caused immediate large ST-segment elevations with associated cardiogenic shock; mean arterial pressure (MAP) dropped from 60mmHg to 40mmHg. Dopamine infusion 3ug/kg/min was started to maintain blood pressure. The balloon was readjusted to mid-LAD for the remainder of the 90 minutes. During reperfusion, the animal went into sustained VT requiring direct current cardioversion (DCCV). It was continued on lidocaine infusion 20ug/kg/min for the next 24 hours without further evidence of arrhythmias or hemodynamic compromise.

P13—This animal was planned for ischemia by balloon occlusion in the mid-LAD for 90. After initial inflation the balloon, there was immediate ST-segment elevatiosn seen across all precordial leads on ECG. After the balloon had been up for 85 minutes, the subject became hemodynamically unstable with sudden drop in blood pressure leading ventricular fibrillation (VF) alternating with VT. CPR was initiated; shocks were delivered per ACLS protocol. Epinephrine 1mg IV bolus was given, dopamine infusion was started, amiodarone IV bolus was given due to refractory VF/VT. At the 90-min time point, the balloon was deflated and removed. After 30 minutes of CPR, the subject regained spontaneous circulation; ECG showed sinus tachycardia. Lidocaine, amiodarone 75mg, dopamine 10ug/kg/min was continued for 24 hours. The next day on rounds, the subject had peripheral and dependent pitting edema, for which Lasix 1/g/kg IV twice daily was started for 2 days. Dopamine 10ug/kg/min was continued for another 24 hours.

P14—The balloon was inflated in the mid-LAD for 180 minutes with associated ST-elevation but without hemodynamic instability or arrhythmias. Subject became apneic and hypercapnic from over-sedation but quickly resumed spontaneous breathing with normal CO2 after decreasing sedation. There were no further complications through the recovery of the subject after the procedure.

P15—The balloon was inflated in the mid-LAD for 180 minutes. There were frequent PVCs, but no ventricular tachycardia or fibrillation observed during LAD ischemia and reperfusion. There were no hemodynamic complications throughout the procedure.

P16—The balloon was inflated in the mid-LAD for 180 minutes. No ventricular arrhythmias occurred during the infarct procedure. No reperfusion-related arrhythmias occurred. Intermittent hypotension episodes during infarct procedure occurred that were responsive to 25–50cc saline boluses. Blood pressure was adequate post infarct surgery without any further intervention.

P17—The balloon was inflated in the mid-LAD for 180 minutes. There was no ventricular tachycardia/fibrillation or hypotension during infarction or reperfusion. There were no reperfusion arrhythmias observed.

P18—The balloon was inflated in the mid-LAD for 180 minutes. During inflation of the angioplasty balloon, the animal was found to be in cardiogenic shock, with systolic BP ~50mmHg. Dobutamine infusion was started and the balloon was repositioned more distally with improvement of the blood pressure. The balloon occlusion was completed after the typical 180 minutes, during which no further episodes of hypotension nor ventricular arrhythmias were observed. The right femoral artery, the location of the arterial cut-down for sheath placement, had a tear that was too large for primary repair. The right femoral vein was harvested to use as a bypass graft. Distal arterial flow and perfusion were confirmed after the procedure.

P19—The balloon was placed at a proximal to mid-LAD position with subsequent hypotension (MAPs <50mmHg) unresponsive to IV fluid bolus. The balloon was repositioned to the mid-LAD with resolution of the hypotension. After 2 hours of ischemia, the animal went into VT with MAP <50mmHg), requiring 2 rounds of CPR and DCCV before return of spontaneous circulation. The artery was reperfused at 3 hours. There were no further complications through the rest of the procedure or recovery.

P20—The animal underwent the usual protocol for ischemia-reperfusion (mid-LAD occlusion, 180 minutes) without significant ST elevations but did develop new q-waves in V1–4. No other complications were noted through the rest of the procedure and recovery.

P20.5—The balloon was inflated in the mid-LAD for 180 minutes without arrhythmias, but the animal developed mild hypotension that was responsive to fluid boluses. After reperfusion, there were no arrhythmias noted, and the subject recovered without complications. The next morning, the animal collapsed during rounds and was unresponsive. An emergent ECG demonstrated ventricular fibrillation (HR >300bpm). CPR was performed

for 8 rounds without improvement or return of spontaneous circulation. The attending veterinarian declared the subject expired and a necropsy was performed.

P21—Engagement of the left coronary artery with the guide catheter was difficult and required an extended amount of time and contrast to position the balloon in the mid-LAD. Upon inflation, the animal's blood pressure dropped, responding to intermittent fluid boluses during the 180 minutes of ischemia. After deflating the balloon, the initial observed rhythm was AIVR with HR ~160 bpm, but converted to normal sinus rhythm after 2 minutes. Subject was found to have an estimated left ventricular ejection fraction of ~40% per cage-side echo with intermittent non-sustained VT. The subject was given a 2 days course of IV Lasix, lidocaine infusion and dobutamine infusion.

P22—Frequent PVCs were observed immediately after the balloon was inflated in the mid-LAD. About an hour after inflation, the subject's blood pressure dropped with significant global hypokinesis and LV dilation by fluoroscopy. The guide catheter was felt to be too close to the aortic valve and causing severe aortic regurgitation. Once the catheter was pulled back, the hemodynamics improved with sustained MAP of 65mmHg for the rest of the procedure. During reperfusion, no arrhythmias were noted. During recover, a non-sustained episode of VT was seen on telemetry; the animal was asymptomatic. The day after the procedure, the animal was found to have a large groin hematoma, with a low hemoglobin count thought to be from a continued oozing from surgical site, requiring a blood transfusion. No vascular compromise was seen; distal perfusion was preserved. Blood count and hematoma size were stable the following days.

P23—The balloon was inflated in the mid-LAD for 180 minutes followed by reperfusion. There were no hemodynamic complications or arrhythmias were noted during the procedure.

P24—The balloon was inflated in the mid-LAD for 180 minutes. After the inflation of the balloon, the subject immediately developed hypotension that was not responsive to fluid boluses. Dopamine infusion was started to maintain an MAP >60mmHg. The guide catheter tip was noted to be pinning one of the aortic valve cusps, causing severe aortic regurgitation. Blood pressure improved after pulling back the catheter tip. During the removal of the balloon after deflation, the guide catheter became deeply seated in the LAD, leading to asystole and loss of blood pressure on invasive blood pressure monitoring. The catheter, wires and balloon were removed, CPR was initiated with return of spontaneous circulation after 2 rounds. The immediate rhythm was AIVR with HR of 150bpm and converted into normal sinus rhythm after 2 minutes with normal blood pressure.

P25—The balloon was inflated in the mid-LAD for 180 minutes. During the procedure, there was intermittent hypotension but with MAP >60mmHg, no inotrope or fluid boluses were given. After removal of the balloon, there was AIVR with rate of ~170bpm for about 2 minutes, after which the heart returned to normal sinus rhythm. There were no further complications through post-procedure recovery.

P32—The balloon was inflated in the mid-LAD for 180 minutes. There were no arrhythmias during infarction or reperfusion. The animal developed hypotension

(~50mmHg) 5min after balloon inflation, which was responsive to 50cc saline bolus. There were no further complications through post-procedure recovery. However, the animal developed ventricular tachycardia with a rate of ~250 bpm starting one week after cell transplant, and the animal became lethargic with heart rate of ~300 bpm 1 month after cell transplant. Because of the persistent tachycardia, no MRI scans were possible.

P39—The balloon was inflated in the mid-LAD for 180 minutes without arrhythmias. After removal of the balloon, there were frequent PVCs for 5min which returned to normal sinus rhythm without any intervention. The animal was hemodynamically stable throughout the procedure. There were no further complications through post-procedure recovery.

Supplementary Material

Refer to Web version on PubMed Central for supplementary material.

Acknowledgments

These studies were supported in part by NIH Grants R01HL128362, R01 HL084642, P01HL094374, and a grant from the Fondation Leducq Transatlantic Network of Excellence (all to CEM). These studies also were supported by the UW Medicine Heart Regeneration Program, the Washington Research Foundation, and a gift from Mike and Lynn Garvey. The manufacture of cells provided by City of Hope was funded in part through the National Heart Lung and Blood Institute's Production Assistance for Cell Therapies (PACT). We also acknowledge the support of the Cell Analysis Facility Flow Cytometry and Imaging Core in the Department of Immunology at the University of Washington. We thank the Garvey Imaging Core for assistance with microscopy. We are indebted to the dedicated staff of the Washington National Primate Research Center for supporting many aspects of this study. We thank Dr. Michael Laflamme for helpful discussions, Dr. Wei-Zhong Zhu for support with electrophysiological studies, and Dr. Paul Swanson for consultation on the renal tumor. We thank Drs. Jeffrey Maki and Gregory Wilson for help with cardiac MRI protocol.

Author Contributions

Y-WL designed experiments, conducted animal studies, analyzed data and edited the manuscript.

BC designed experiments, conducted animal studies, performed histology studies, analyzed data and edited the manuscript.

XY performed histology, histomorphometry, analyzed data, prepared figures, and edited the manuscript.

JAF prepared cells for transplantation and edited the manuscript.

FAK prepared cells for transplantation and edited the manuscript.

AF-T prepared cells for transplantation and edited the manuscript.

LC supervised cell manufacturing.

KWV designed experiments, conducted animal studies, and provided veterinary care.

CAA designed experiments and conducted animal studies

AB performed necropsies and provided pathology consultation.

JO conducted animal studies and edited the manuscript

CWD designed experiments, conducted animal studies and edited the manuscript.

ZLS conducted animal studies and edited the manuscript.

SPS designed experiments, conducted electrophysiology studies, analyzed data and edited the manuscript.

SAT conducted animal studies, analyzed data and edited the manuscript.

HT conducted animal studies and edited the manuscript.

AVN performed MRI studies, analyzed data and edited the manuscript.

SKD performed histology.

MSL analyzed MRI scans.

JL analyzed MRI scans and edited the manuscript.

DWH advised on and performed microscopy.

HR designed experiments, performed histology, conducted molecular analyses, analyzed data, and prepared figures.

LP designed experiments, analyzed data and edited the manuscript.

BHF prepared cells for transplantation.

WRM designed experiments, analyzed data and edited the manuscript.

RST designed experiments, conducted animal studies, oversaw preparation of cells for transplantation, analyzed data, prepared figures and edited the manuscript.

CEM supervised all components of this study, designed experiments, performed animal experiments, analyzed data, obtained funding for the study, prepared figures and wrote the manuscript.

References

1. Forouzanfar MH, et al. Assessing the global burden of ischemic heart disease, part 2: analytic methods and estimates of the global epidemiology of ischemic heart disease in 2010. Glob Heart. 7:331–342.2012; [PubMed: 23505617]
2. Laflamme MA, Murry CE. Heart regeneration. Nature. 473:326–335.2011; [PubMed: 21593865]
3. Eschenhagen T, et al. Cardiomyocyte Regeneration: A Consensus Statement. Circulation. 136:680–686.2017; [PubMed: 28684531]
4. Bergmann O, et al. Evidence for cardiomyocyte renewal in humans. Science. 324:98–102.2009; [PubMed: 19342590]

5. Soonpaa MH, Field LJ. Survey of studies examining mammalian cardiomyocyte DNA synthesis. Circ Res. 83:15–26.1998; [PubMed: 9670914]
6. van Berlo JH, et al. c-kit+ cells minimally contribute cardiomyocytes to the heart. Nature. 509:337–341.2014; [PubMed: 24805242]
7. Burridge PW, Sharma A, Wu JC. Genetic and Epigenetic Regulation of Human Cardiac Reprogramming and Differentiation in Regenerative Medicine. Annu Rev Genet. 49:461–484.2015; [PubMed: 26631515]
8. Gerbin KA, Murry CE. The winding road to regenerating the human heart. Cardiovasc Pathol. 24:133–140.2015; [PubMed: 25795463]
9. Lee RT, Walsh K. The Future of Cardiovascular Regenerative Medicine. Circulation. 133:2618–2625.2016; [PubMed: 27324357]
10. Hassink RJ, et al. Cardiomyocyte cell cycle activation improves cardiac function after myocardial infarction. Cardiovasc Res. 78:18–25.2008; [PubMed: 18079102]
11. Xin M, et al. Hippo pathway effector Yap promotes cardiac regeneration. Proc Natl Acad Sci U S A. 110:13839–13844.2013; [PubMed: 23918388]
12. Heallen T, et al. Hippo signaling impedes adult heart regeneration. Development. 140:4683–4690.2013; [PubMed: 24255096]
13. Heallen T, et al. Hippo pathway inhibits Wnt signaling to restrain cardiomyocyte proliferation and heart size. Science. 332:458–461.2011; [PubMed: 21512031]
14. Shapiro SD, et al. Cyclin A2 induces cardiac regeneration after myocardial infarction through cytokinesis of adult cardiomyocytes. Sci Transl Med. 6:224ra227.2014;
15. Leach JP, et al. Hippo pathway deficiency reverses systolic heart failure after infarction. Nature. 550:260–264.2017; [PubMed: 28976966]
16. Liu Z, et al. Single-cell transcriptomics reconstructs fate conversion from fibroblast to cardiomyocyte. Nature. 551:100–104.2017; [PubMed: 29072293]
17. Zhou H, et al. ZNF281 enhances cardiac reprogramming by modulating cardiac and inflammatory gene expression. Genes Dev. 31:1770–1783.2017; [PubMed: 28982760]
18. Cao N, et al. Conversion of human fibroblasts into functional cardiomyocytes by small molecules. Science. 352:1216–1220.2016; [PubMed: 27127239]
19. Kadota S, Pabon L, Reinecke H, Murry CE. In Vivo Maturation of Human Induced Pluripotent Stem Cell-Derived Cardiomyocytes in Neonatal and Adult Rat Hearts. Stem cell reports. 8:278–289.2017; [PubMed: 28065644]
20. Cho GS, et al. Neonatal Transplantation Confers Maturation of PSC-Derived Cardiomyocytes Conducive to Modeling Cardiomyopathy. Cell Rep. 18:571–582.2017; [PubMed: 28076798]
21. van Laake LW, et al. Human embryonic stem cell-derived cardiomyocytes survive and mature in the mouse heart and transiently improve function after myocardial infarction. Stem Cell Res. 2007
22. Laflamme MA, et al. Cardiomyocytes derived from human embryonic stem cells in pro-survival factors enhance function of infarcted rat hearts. Nat Biotechnol. 25:1015–1024.2007; [PubMed: 17721512]
23. Caspi O, et al. Transplantation of human embryonic stem cell-derived cardiomyocytes improves myocardial performance in infarcted rat hearts. J Am Coll Cardiol. 50:1884–1893.2007; [PubMed: 17980256]
24. Shiba Y, et al. Human ES-cell-derived cardiomyocytes electrically couple and suppress arrhythmias in injured hearts. Nature. 489:322–325.2012; [PubMed: 22864415]
25. Chong JJ, et al. Human embryonic-stem-cell-derived cardiomyocytes regenerate non-human primate hearts. Nature. 510:273–277.2014; [PubMed: 24776797]
26. Shiba Y, et al. Allogeneic transplantation of iPS cell-derived cardiomyocytes regenerates primate hearts. Nature. 538:388–391.2016; [PubMed: 27723741]
27. Naumova AV, Modo M, Moore A, Murry CE, Frank JA. Clinical imaging in regenerative medicine. Nat Biotechnol. 32:804–818.2014; [PubMed: 25093889]
28. Zhang WY, Ebert AD, Narula J, Wu JC. Imaging cardiac stem cell therapy: translations to human clinical studies. J Cardiovasc Transl Res. 4:514–522.2011; [PubMed: 21538182]

29. Chen VC, et al. Development of a scalable suspension culture for cardiac differentiation from human pluripotent stem cells. Stem Cell Res. 15:365–375.2015; [PubMed: 26318718]
30. Hohnloser SH, Klingenheben T, Singh BN. Amiodarone-associated proarrhythmic effects. A review with special reference to torsade de pointes tachycardia. Ann Intern Med. 121:529–535.1994; [PubMed: 8067651]
31. Chelsky LB, et al. Caffeine and ventricular arrhythmias. An electrophysiological approach. JAMA. 264:2236–2240.1990; [PubMed: 2214101]
32. Nussbaum J, et al. Transplantation of undifferentiated murine embryonic stem cells in the heart: teratoma formation and immune response. Faseb J. 21:1345–1357.2007; [PubMed: 17284483]
33. Kuroda N, Tanaka A, Ohe C, Nagashima Y. Recent advances of immunohistochemistry for diagnosis of renal tumors. Pathol Int. 63:381–390.2013; [PubMed: 23957913]
34. Bedada FB, et al. Acquisition of a quantitative, stoichiometrically conserved ratiometric marker of maturation status in stem cell-derived cardiac myocytes. Stem cell reports. 3:594–605.2014; [PubMed: 25358788]
35. Bergmann O, et al. Identification of cardiomyocyte nuclei and assessment of ploidy for the analysis of cell turnover. Exp Cell Res. 317:188–194.2011; [PubMed: 20828558]
36. Swijnenburg RJ, et al. Embryonic stem cell immunogenicity increases upon differentiation after transplantation into ischemic myocardium. Circulation. 112:I166–172.2005; [PubMed: 16159810]
37. Lee AS, Tang C, Rao MS, Weissman IL, Wu JC. Tumorigenicity as a clinical hurdle for pluripotent stem cell therapies. Nat Med. 19:998–1004.2013; [PubMed: 23921754]
38. Hodgkinson CP, Bareja A, Gomez JA, Dzau VJ. Emerging Concepts in Paracrine Mechanisms in Regenerative Cardiovascular Medicine and Biology. Circ Res. 118:95–107.2016; [PubMed: 26837742]
39. Gerbin KA, Yang X, Murry CE, Coulombe KL. Enhanced Electrical Integration of Engineered Human Myocardium via Intramyocardial versus Epicardial Delivery in Infarcted Rat Hearts. PLoS One. 10:e0131446.2015; [PubMed: 26161513]
40. Zhu K, et al. Lack of Remuscularization Following Transplantation of Human Embryonic Stem Cell-Derived Cardiovascular Progenitor Cells in Infarcted Nonhuman Primates. Circ Res. 2018
41. Tachibana A, et al. Paracrine Effects of the Pluripotent Stem Cell-Derived Cardiac Myocytes Salvage the Injured Myocardium. Circ Res. 121:e22–e36.2017; [PubMed: 28743804]
42. Liao SY, et al. Overexpression of Kir2.1 channel in embryonic stem cell-derived cardiomyocytes attenuates posttransplantation proarrhythmic risk in myocardial infarction. Heart Rhythm. 10:273–282.2013; [PubMed: 23041574]
43. Liao SY, et al. Proarrhythmic risk of embryonic stem cell-derived cardiomyocyte transplantation in infarcted myocardium. Heart Rhythm. 7:1852–1859.2010; [PubMed: 20833268]
44. Roell W, et al. Engraftment of connexin 43-expressing cells prevents post-infarct arrhythmia. Nature. 450:819–824.2007; [PubMed: 18064002]
45. Chong JJ, Murry CE. Cardiac regeneration using pluripotent stem cells-Progression to large animal models. Stem Cell Res. 2014
46. Fernandes S, et al. Human embryonic stem cell-derived cardiomyocytes engraft but do not alter cardiac remodeling after chronic infarction in rats. J Mol Cell Cardiol. 49:941–949.2010; [PubMed: 20854826]

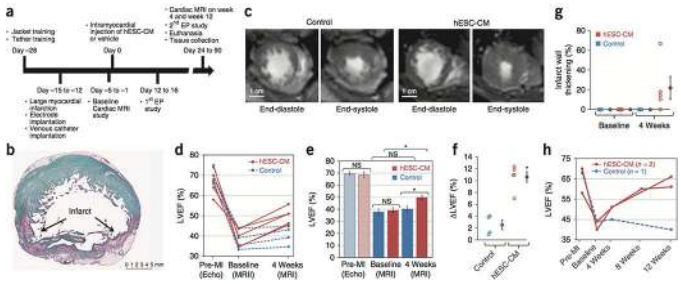

Figure 1. Effects of hESC-CM Transplantation on Cardiac Function

(a) Timeline for the efficacy study in which non-human primates received 180 minute ischemia/reperfusion in the mid LAD vascular bed. Cardiac MRI is incorporated to measure cardiac dimensions and function. Electrophysiology studies are also included in the protocol to study the cause, inducibility, and severity of the ventricular arrhythmias. **(b)** A representative stain of a short-axis cross section of an infarcted NHP control heart with picrosirius red and fast green, where the infarct collagen is red and healthy myocardium is green. The infarct is transmural, with sparing of subendocardial myocardium. These experiments were repeated 4 times for controls and 5 times for hESC-CM treatment, with similar results. Scale bar, 5 mm. **(c)** Representative short-axis CINE MRI at end-diastolic and end-systolic phases of the cardiac cycle at 4 weeks after treatment (6 weeks after MI). Blood in the chamber appears bright. There is greater ejection of blood in the hESC-CM heart during systole. These experiments were repeated 4 times for controls and 5 times for hESC-CM treatment, with similar results. Scale bar, 1 cm. **(d)** Plot of left ventricular ejection fraction (LVEF) for individual subjects (4 control animals, blue; 5 hESC-CM treated animals, red) prior to infarction (Pre-MI), at the post-infarction baseline (one day prior to injection) and at 1 month post treatment. All hESC-CM hearts show significant improvement, while there is minimal improvement in controls. (**e**) Mean LVEF is comparable between groups prior to infarction and at post-infarction baseline but shows a significant improvement after hESC-CM treatment (*P=0.004, paired t-test, df=4). Data are from 4 biologically independent control animals and 5 hESC-CM treated animals. Bars represent mean ± SEM. Individual data points are shown in 1d. **(f)** Change in LVEF (ΔLVEF) from baseline to 4 weeks is significantly greater in hESC-CM hearts than in controls Data are from 4 biologically independent control animals and 5 hESC-CM treated animals. Bars represent mean ± SEM. (*P=0.004, 2-tailed t-test, df=7). (**g**) There is a variable trend (P=0.135, paired t-test, df=7) 4) toward increased systolic thickening of the infarcted wall in hESC-CM treated animals. Data are from 4 biologically independent control animals and 5 hESC-CM treated animals. Bars represent mean ± SEM. **(h)** Extending survival to 12 weeks demonstrates a modest reduction in LVEF in control hearts and further improvement with hESC-CM treatment. This suggests the benefits seen at 4 weeks are stable with the potential for substantial further improvement.

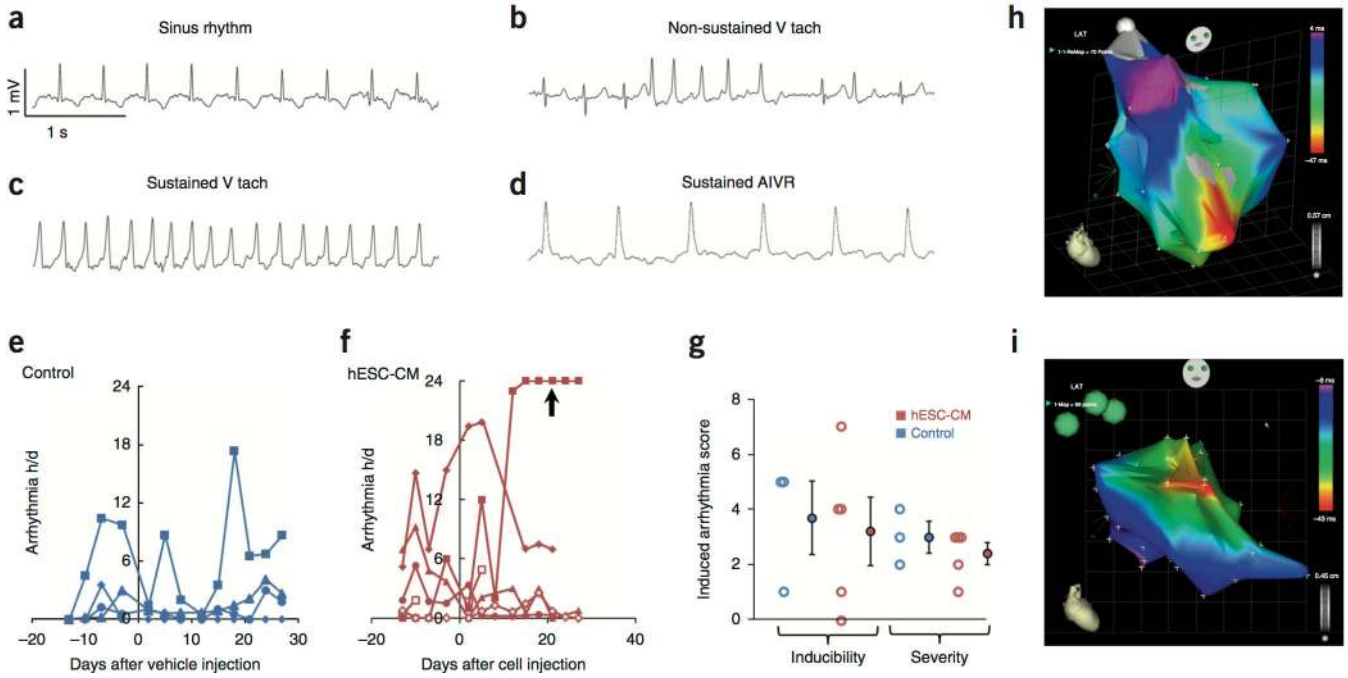

Figure 2. Analysis of Arrhythmias

(a–d) Electrocardiograms from telemetry analysis of 4 biologically independent control animals and 5 hESC-CM treated animals demonstrating normal sinus rhythm (**a**), non-sustained ventricular tachycardia (**b**), sustained ventricular tachycardia (**c**), and sustained accelerated idioventricular rhythm (**d**). (**e, f**) Spontaneous ventricular arrhythmias in large infarct protocol (3-hour mid-LAD occlusion) for 4 biologically independent control animals **(e)** and 5 individual control **(e)** and hESC-CM treated animals **(f)** were recorded as hours/day (24hrs). Both groups have ventricular arrhythmias before and after injection (day 0), but the hESC-CM group had one subject with protracted arrhythmias (arrow), that likely are treatment-related. **(g)** Programmed electrical stimulation studies demonstrate that the inducibility and severity between biologically independent control (N=3) and hESC-CM treated hearts (N=5) were not significantly different(P=0.816, 2-tailed t-test, df=6 for inducibility; P=0.411, 2-tailed t-test, df=6 for severity). Group data indicate mean ± SEM. **(h, i)** Electrical activation maps acquired using an endocardial catheter electrode. Red = early activation; magenta = late activation **(h)** Activation in a non-infarcted macaque heart initiates at the apex (red; pointing toward the observer) and spreads toward the base. N=1. **(i)** Activation map from an hESC-CM-engrafted heart during spontaneous ventricular tachycardia, with apex pointing toward lower right. Activation originates from an apparent point source in the anterior septum. No rotor was identified. This experiment was independently repeated twice with similar results.

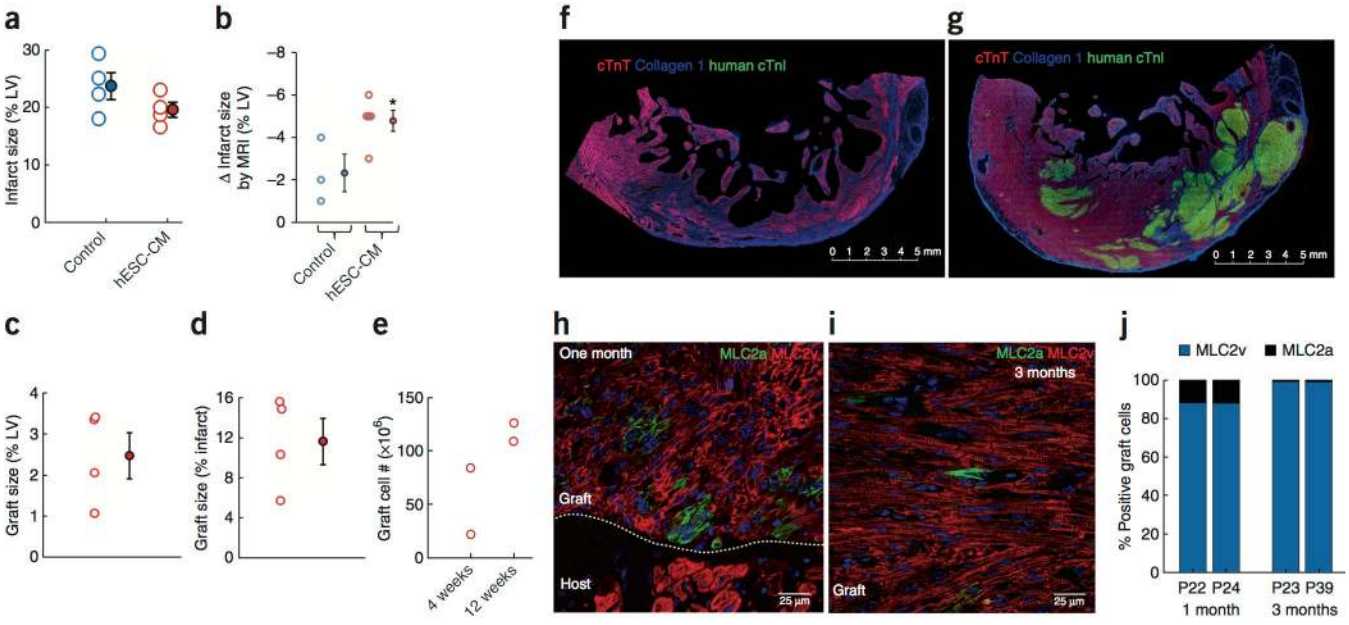

Figure 3. Structural assessment of infarct, graft size and graft composition

(a) Histological infarct size was not different between groups at the end of the study. Each point is one heart. Data are from 4 biologically independent control animals and 5 hESC-CM treated animals. Group data are means ± SEM. **(b)** Scar shrinkage by MRI from baseline to 4 weeks was significantly greater in hESC-CM hearts. Group data are means ± SEM. **(c, d)** Histological graft size expressed as a percentage of left ventricle and of the infarct. Data are from 4 biologically independent hESC-CM treated animals. Group data are means ± SEM. **(e)** Graft cell number determined by histomorphometry. Note the increase in cell number from 4 to 12 weeks. Each point represents 1 heart, with 2 biologically independent replicates at each of 4 and 12 weeks. **(f, g)** Low magnification immunofluorescent images stained for cardiac troponin T (cTnT; red; human + monkey myocardium), human-specific cardiac troponin I (human cTnI; green; human myocardium) and type I collagen to identify scar tissue (blue). **(f)** Control heart showing transmural infarct and lateral border zone. Note the spared host subendocardial myocardium and the thinned infarct wall compared to the border zone. This experiment was repeated in 4 biologically independent control animals with similar results. Scale bar, 5 mm. **(g)** hESC-CM engrafted heart showing large islands of human myocardium (green) within the infarct and lateral border zone. Note the relative preservation of wall thickness in the infarct region. This experiment was repeated in 5 biologically independent hESC-CM treated hearts, with similar results in 4. In 1 animal the graft was lost after 4 weeks due to interruption of immunosuppression. Scale bar, 5 mm. **(h, i)** Graft staining for definitive ventricular phenotype (MLC2v, red) or immature ventricular/atrial/nodal cardiomyocyte phenotype (MLC2a, green). **(h)** At 1 month post-engraftment, the majority of graft cells express MLC2v, but MLC2a$^+$ cells are readily identified. Note that host cardiomyocytes express only MLC2v. This experiment was repeated in 2 biologically independent hESC-CM treated hearts, with similar results. Scale bar, 25 μm. **(i)** At 3 months post-engraftment the graft is comprised almost entirely of definitive ventricular cardiomyocytes, and only rare MLC2a$^+$ cells can be identified. This experiment was repeated in 2 biologically independent hESC-

CM treated hearts, with similar results. Scale bar, 25 μm. **(j)** Quantitation of MLC2v and MLC2a staining. At 3 months both grafts are 99% MLC2v^{+}. Each bar represents 1 animal.

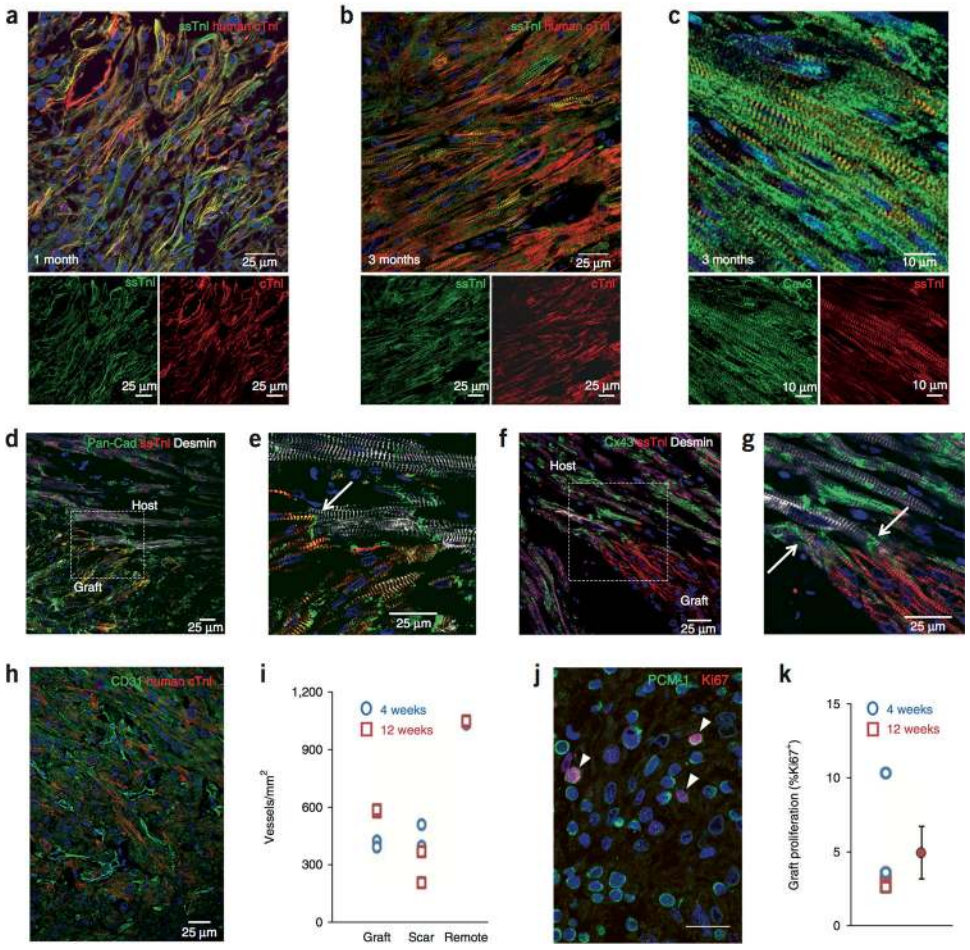

Figure 4. Graft maturation, integration, vascularization and proliferation

(a, b) hESC-CM grafts stained for slow skeletal troponin I (ssTnI, green) and human cardiac troponin I (cTnI, red). Merged image on top, individual channels below. Scale bar, 25 μm. **(a)** At 1 month the hESC-CMs are relatively small, have peripheral myofibrils and exhibit low cellular alignment. Low level expression of cTnI is evident. This experiment was repeated in 2 biologically independent hESC-CM treated hearts with similar results. **(b)** At 3 months the cells have hypertrophied, have myofibrils throughout the cytoplasm and are better aligned. Increased expression of cTnI is evident. This experiment was repeated in 2 biologically independent hESC-CM treated hearts with similar results. **(c)** At 3 months, graft T-tubule networks are present, shown by caveolin-3 staining (Cav3, green). ssTnI, red. This experiment was repeated in 2 biologically independent hESC-CM treated hearts with similar results. Scale bar, 10 μm. **(d)** Interface of 3-month graft and host myocardium stained for pan-cadherin (green), ssTnI (human graft, red) and desmin (graft + host, white). This experiment was repeated in 2 biologically independent hESC-CM treated hearts with similar results. Scale bar, 25 μm. **(e)** Magnified image of region boxed in (d) demonstrates cadherin-positive adherens junction at intercalated disk between graft and host (arrow). This experiment was repeated in 2 biologically independent hESC-CM treated hearts with similar results. Scale bar, 25 μm. **(f)** Interface of 3-month graft and host myocardium stained for connexin43 (Cx43, green), ssTnI (human graft, red) and desmin (graft + host, white). This

experiment was repeated in 2 biologically independent hESC-CM treated hearts with similar results. Scale bar, 25 μm. **(g)** Magnified image of region boxed in (f) demonstrates connexin43-positive gap junctions at intercalated disks between graft and host (arrows). This experiment was repeated in 2 biologically independent hESC-CM treated hearts with similar results. Scale bar, 25 μm. **(h)** Vascularization of the human myocardium (human cTnI-positive, red) by host microvessels is demonstrated by staining endothelial cells for CD31 (green). This experiment was repeated in 4 biologically independent hESC-CM treated hearts with similar results. Scale bar, 25 μm. **(i)** Quantitation of vascular density in graft, scar and remote myocardium at 4 and 12 weeks. Each point is 1 heart. Data are from 4 biologically independent control animals and 4 hESC-CM treated animals. **(j)** Proliferation of 4-week hESC-CM graft demonstrated by staining for pericentriolar material-1 (PCM-1; green) and Ki67 (red). Cardiomyocyte nuclei in cell cycle are indicated by arrowheads. This experiment was repeated in 4 biologically independent hESC-CM treated hearts with similar results. Scale bar, 20 μm. **(k)** Quantitation of graft cardiomyocyte proliferation at 4 weeks and 12 weeks. Each point is 1 heart. Data are from 2 biologically independent hESC-CM treated hearts each at 2 and 4 weeks. Group data are mean ± SEM for all 4 hearts.

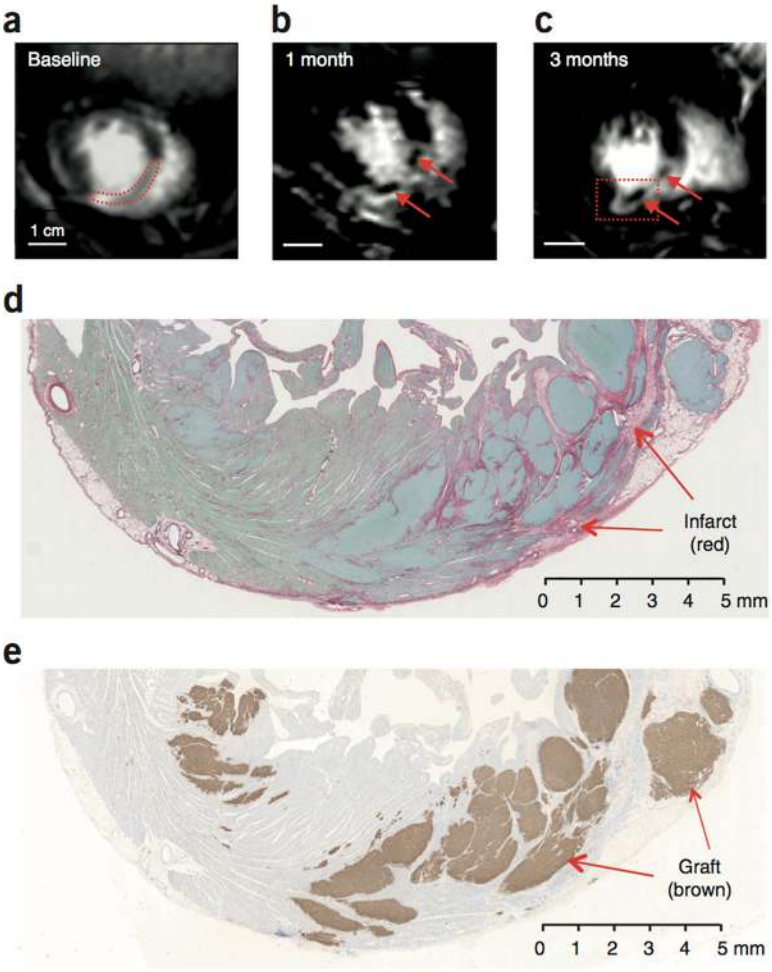

Figure 5.

Visualization of grafts by MRI. (a–c) Delayed Gd enhanced MR images of macaque heart to identify the infarct scar. Blood in the chambers appears bright. Viable myocardium appears dark, and infarcted tissue appears light gray. The same short-axis region of the heart is shown in each scan. (a) At baseline, the infarct is a homogeneous tissue located in the anterior wall and interventricular septum (outlined by red dotted line). (b, c) At 1 month and 3 months post-engraftment, new areas of viable dark (Gd-negative) tissue appear within the infarct (arrows). (d) Histological section corresponding to the region boxed in (c) stained with picrosirius red to identify collagen and fast green to identify myocardium. Infarct scar is readily identifiable as red tissue, but it contains islands of green tissue consistent with myocardium. Scale bar, 5 mm. (e) Adjacent section from region boxed in (c) stained for human cTnT (brown) to identify human myocardial graft. There is extensive human myocardium within the infarct and in the lateral border zone, measuring >1 cm in maximal dimension. Note that human myocardium within the scar would be visible by MRI, but grafts in the border zone host myocardium would be MRI-invisible, since both exclude Gd. This experiment was repeated 4 times with biologically independent hESC-CM treated

animals, with similar results found in 3. In 1 animal, the graft could not reliably be distinguished by MRI.

Table 1

Data for individual macaques in MRI study [AU: Provide table in normal black font without colors]

							Pre-Infarction	Post-Infarction Baseline MRI					MRI 4 weeks after treatment				
Animal #	**Sex**	**Age**	**Weight, kg**	**Infarct size (histology), % of LV**	**Graft size, % of infarct**	**Graft cell number (millions)**	**LVEF by Echo, %**	**LVEDV, ml**	**LVESV, ml**	**LVEF, %**	**Infarcted LVTh, %**	**Infarct size, % of LV**	**LVEDV, ml**	**LVESV, ml**	**LVEF, %**	**Infarcted LVTh, %**	**Infarct size, % of LV**
			Control														
P14	M	6y 10mo	12.6	29.2	NA	NA	68	18.0	10.2	43.9	0	19	20.7	11.4	44.8	0	18
P15	F	9y 7mo	11.7	22.2	NA	NA	74	19.0	11.6	39.1	0	NA	23.6	13.4	43.1	0	NA
P18	F	10y 9mo	11.4	18.1	NA	NA	67	16.1	10.7	33.4	0	15	18.3	11.9	34.7	0	13
P20	F	6y 0mo	10.6	25.0	NA	NA	70	15.5	10.0	35.5	0	17	13.0	7.9	39.3	0	13
Mean		**8**	**11.6**	**23.6**	**NA**	**NA**	**69.8**	**17.2**	**10.6**	**38.0**	**0**	**17**	**18.9**	**11.2**	**40.5**	**0**	**15**
SEM		**1**	**0.4**	**2.3**	**NA**	**NA**	**1.3**	**0.8**	**0.4**	**2.3**	**0**	**1**	**2.2**	**1.2**	**2.2**	**0**	**1**
			hESC-CM														
P22	F	15y 7mo	7.0	18.7	5.7	23.0	75	13.2	8.6	34.5	0	31	12.3	6.6	46.3	14	26
P23	F	11y 6mo	10.7	23.0	14.8	133.6	70	16.1	9.6	40.1	0	15	13.3	6.5	51.1	67	10
P24	F	12y 2mo	9.5	19.9	10.3	88.9	66	15.2	9.9	34.7	0	25	16.1	8.8	45.6	0	20
P25	F	6y 7mo	5.2	16.6	ND	ND	64	11.7	6.6	43.5	0	17	13.8	6.1	55.8	10	11
P39	F	14y 6 mo	9.2	21.5	15.6	115.6	58	13.7	7.6	44.0	0	16	11.2	5.5	51.0	18	13
Mean		**11**	**8.6**	**19.9**	**11.6**	**90.3**	**66.6**	**14.0** *	**8.5** *	**39.4**	**0**	**21**	**13.3** *	**6.7** **	**50.0** *	**22**	**16**
SEM		**2**	**0.9**	**1.1**	**2.3**	**21.0**	**2.9**	**0.8**	**0.6**	**2.1**	**0**	**3**	**0.8**	**0.6**	**1.9**	**12**	**3**

All hESC-CMs for these studies were derived from the H7 line.

NA, not applicable or not available

ND, Not detected. Graft was rejected at 5 weeks post-engraftment due to damage to intravenous catheter and interruption of immunosuppression. Not included in graft size calculations.

Infarcted LVTh, infarcted left ventricular wall systolic thickening

* p< 0.05 control vs. hESC-CM treated

** p < 0.01 control vs. hESC-CM treated